ADVANCED MATERIALS INTERFACES
Open Access
www.advmatinterfaces.de

N-Heterocyclic Olefins on a Metallic Surface – Adsorption, Orientation, and Electronic Influence

Felix Landwehr, Mowpriya Das, Sergio Tosoni, Juan J. Navarro, Ankita Das, Maximilian Koy, Markus Heyde,* Gianfranco Pacchioni, Frank Glorius,* and Beatriz Roldan Cuenya*

N-Heterocyclic olefins (NHOs), possessing highly polarizable and remarkably electron-rich double bonds, have been effectively utilized as exceptional anchors for surface modifications. Herein, the adsorption, orientation, and electronic properties of NHOs on a metal surface are investigated. On Cu(111), the sterically low-demanding IMe-NHO is compared to its analogous IMe-NHC counterpart. High-resolution electron energy-loss spectroscopy (HREELS) measurements show for both molecules a flat-lying ring adsorption configuration. While the NHC adopts a dimer configuration including a Cu adatom, the NHO chemisorbs over a C–Cu bond perpendicular to the surface. This distinct difference leads for the IMe-NHOs to have a higher thermal stability on the surface. Moreover, IMe-NHOs introduce a higher net electron transfer to the surface compared to the IMe-NHCs, which results in a stronger effect on the work function. These results highlight the role of NHOs in surface science as they extend the functionalization capabilities of NHCs into stronger electronic modification.

1. Introduction

Although the inception of N-heterocyclic olefins (NHOs) (ene-1,1-diamines) in literature dates back several decades,[1] those compounds have remained relatively unexplored despite their intriguing nature. However, in recent years, they have been emerging as a captivating class of ligands in organo-catalysis and polymerization reaction.[2] This development parallels the emergence of N-heterocyclic carbenes (NHCs), from which NHOs can formally be derived by addition of a terminal alkylidene moiety.[3] The electron-rich and highly polarizable double bond of NHOs leads to elevated nucleophilicity at the exocyclic carbon center (C_{exo}), which can be rationalized by the ylidic character of NHOs (**Scheme 1a**).[4] This ylidic character leads to a change in the bonding properties in metal complexes making NHOs excellent at binding to electron-rich, low-oxidation state metal species.[5]

After their successful isolation in 1993, NHOs found utility in stabilizing a wide range of transition metals and main group species due to their strong Lewis basic site, thereby pioneering their application in catalysis.[2,3,6–10] Furthermore, NHOs exhibit a structural resemblance to the "deoxy-Breslow" intermediates that arise in specific NHC-organo-catalyzed reactions.[11–15] Initial investigations demonstrate the robust σ-donor capacity of NHOs, accompanied by the absence of π-backbonding characteristics.[5,16,17]

Conversely, in recent years NHCs (Scheme 1b) have garnered significant scientific interest as surface modifications in the fields of material science and catalysis,[18–35] with many studies focusing on the binding and adsorption geometry of NHCs on well-prepared surfaces, such as different crystal facets of Au,[36–45] Si,[46] or Ag.[37] Our groups contributed to this field by elucidating the adsorption geometry of a di-isopropylphenyl-substituted NHC (IPr-NHC) on Cu and oxidized Cu surfaces.[37,47–50] However, surface modification using NHO ligands has remained unexplored on Cu surfaces, presenting an intriguing avenue for investigation.

Given the distinct geometric and electronic properties of NHOs in comparison to NHCs, it is anticipated that surface modifications of NHOs could yield novel properties and assembly behavior which is essential for the potential applications of these promising ligands in material science and catalysis.

Recently, the deposition of NHO species on a Au(111) and a Si(111) surface have been reported.[51,52] These studies have

F. Landwehr, J. J. Navarro, M. Heyde, B. R. Cuenya
Department of Interface Science
Fritz-Haber Institute of the Max Planck Society
Faradayweg 4–6, 14195 Berlin, Germany
E-mail: heyde@fhi.mpg.de
M. Das, A. Das, M. Koy, F. Glorius
Organisch-Chemisches Institut
Westfälische Wilhelms-Universität
Corrensstraße 40, 48149 Münster, Germany
E-mail: glorius@uni-muenster.de
S. Tosoni, G. Pacchioni
Dipartimento di Scienza dei Materiali
Università di Milano-Bicocca
Via Cozzi 55, Milano 20125, Italy
E-mail: sergio.tosoni@unimib.it

The ORCID identification number(s) for the author(s) of this article can be found under https://doi.org/10.1002/admi.202400378

DOI: 10.1002/admi.202400378

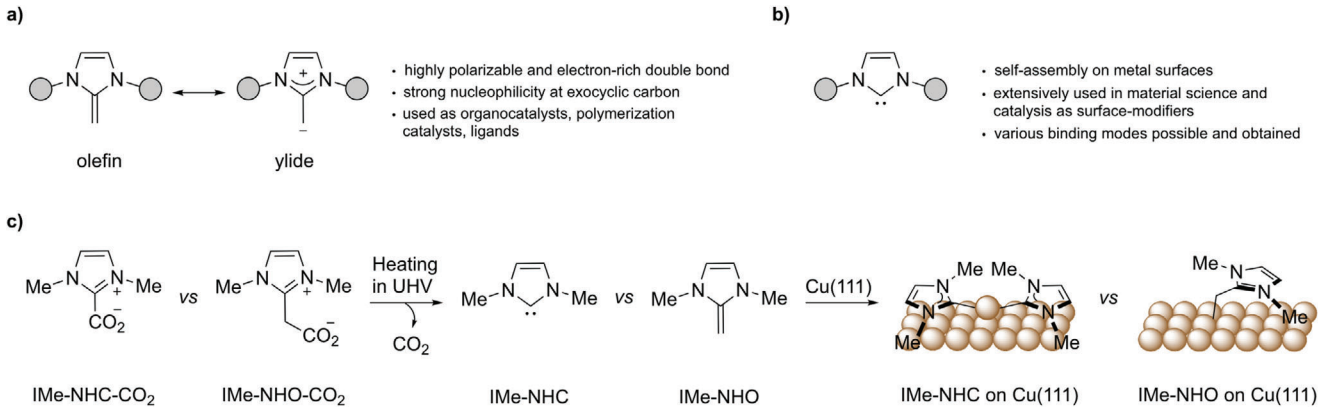

Scheme 1. NHCs and NHOs on metal surfaces a) Mesomeric representation of the NHOs. b) Schematic of a free NHC. These molecules have been discussed with different N-substituents on various surfaces in the literature (see main text). c) The process of the UHV introduction and subsequent deposition of 1,3-dimethyl-2,3-dihydro-1*H*-imidazole (IMe-NHC) and 1,3-dimethyl-2-methylidene-2,3-dihydro-1*H*-imidazole (IMe-NHO) on Cu(111) is illustrated.

shown that NHOs bind to the respective surfaces in different ways: while NHOs bind directly to the Si(111) surface, on Au(111) they are believed to adopt an adatom configuration similar to previously reported NHCs.[36,37,47]

In this study, we focused on the deposition of NHC and NHO molecules with small methyl substituents (IMe-NHC and IMe-NHO, respectively) on an ultrahigh vacuum (UHV)-prepared Cu(111) single crystal (Scheme 1c). Cu has been chosen as a substrate because copper has seen an increasing interest in recent years in fields such as microelectronics,[53] photocatalysis[54] and electrocatalysis[55] for its relative abundance and low cost compared to more established materials.[56] Thus, the investigation of the molecule–surface interaction on copper is crucial to develop surface modifiers for practical applications in the mentioned fields.

To ensure stability and ease of handling, we utilized the CO_2 adducts of the molecules as precursors, a common approach in surface science studies involving NHCs.[36,38,46–48] The application of thermal energy would trigger decarboxylation, resulting in the release of the free molecules for vapor deposition onto the intended surface yielding clean, salt-free NHC and NHO under UHV conditions.

We employed low-temperature scanning tunneling microscopy (LT-STM) to investigate the molecular arrangement, high-resolution electron energy-loss spectroscopy (HREELS) to investigate the adsorption geometry and orientation, and X-ray photoemission spectroscopy (XPS) to gain insight into the electronic properties, complemented by density-functional theory (DFT) calculations.

2. Results and Discussion

As a starting point, IMe-NHC and IMe-NHO were deposited on Cu(111) following the procedure described above to obtain low-coverage films (for details, see Section 1, Supporting Information). O1s XPS data as well as push-rod mass spectrometry data confirm that the CO_2-adduct can be used for both IMe-NHC and IMe-NHO (Figures S3 and S7, Supporting Information), as evidenced by the absence of any oxygen signal in the XPS spectra and the absence of the $[NHO+CO_2]^+$ mass fragment.

In the case of IMe-NHC, LT-STM images reveal a nonordered arrangement of the molecules (**Figure 1a**). At full monolayer and multilayer coverage IMe-NHC adsorbs in ordered domains on Cu(111).[37] This is not the case at lower coverages as shown in Figure 1a. This leads us to believe that the reported ordering observed at higher monolayer and multilayer coverages is likely due to constraint effects. However, we are able to observe elongated and triangular structures (1b). This indicates the formation of dimeric and trimeric adatom complexes, as reported in the literature,[36,37] even at low molecular coverages. DFT structural optimization of IMe-NHC on Cu(111) also show that the $(NHC)_2$-Cu_{ad}/Cu(111) is energetically favored.

In the case of IMe-NHO, a similar arrangement with almost no long-range or short-range ordering was observed (Figure 1d,e). DFT calculations reveal an elongation of the C–C bond by 0.06 Å upon binding and a C–Cu bond length of 2.11 Å. The C_{exo} atom adopts the geometry of a distorted tetrahedron with the H–C–H angle at 113.1° and the H–C–Cu angle at 105.4°. This shows a sp^2 to sp^3 transition of the C_{exo}, indicating IMe-NHOs chemisorbs to the surface. It is important to note that IMe-NHO at this point does not seem to adopt the adatom configuration that has been observed for IMe-NHC as confirmed by DFT structural optimization of IMe-NHO on Cu(111). Here, the formation of a (NHO)-Cu_{ad}/Cu(111) adatom complex was found to be thermodynamically unfavorable and kinetically hindered by 1.10 and 1.29 eV, respectively. Moreover, the formation of $(NHO)_2$-Cu_{ad}/Cu(111) dimer complexes could not be observed at all due to sterical hinderance. More details can be found in Figure S9 and Tables S3 and S4, Supporting Information.

These results indicate that there is no intrinsic driving force for self-assembly at low coverage for both molecules, which differs from other NHCs that have been reported[47] (for further details, see Sections 3 and 4, Supporting Information). The lack of self-assembly was also true at elevated temperatures (Figure S6, Supporting Information).

Further analysis based solely on LT-STM data proved to be challenging as commonly employed strategies, such as comparing apparent height of the observed molecules did not lead to any conclusive results.

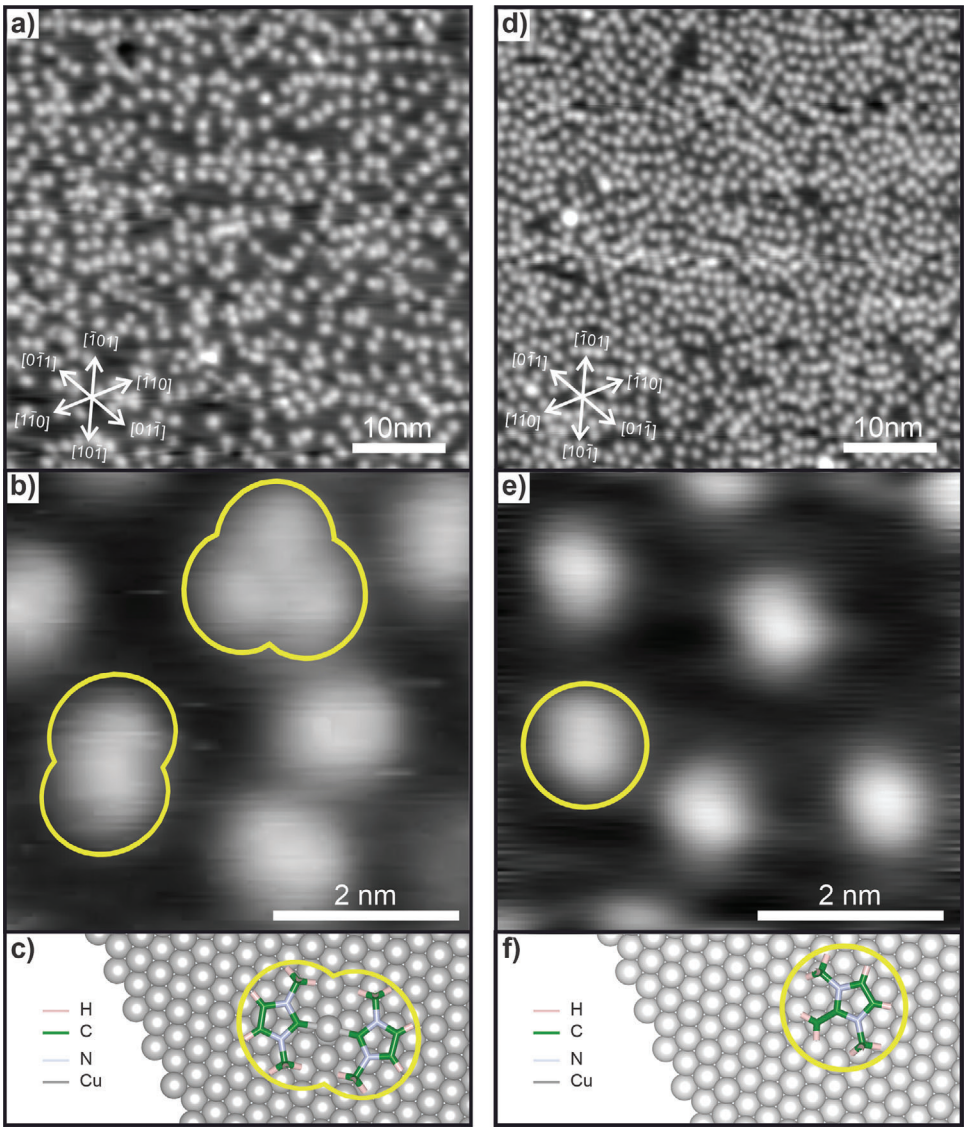

Figure 1. LT-STM (T = 5 K) 50 nm × 50 nm images on Cu(111) of high-sub-monolayer coverages for a) IMe-NHC ($V_s = -1.7$ V and $I_t = 50$ pA) and d) IMe-NHO ($V_s = -1.2$ V and $I_t = 35$ pA). The white lines represent the orientation of the Cu(111) crystal. b, e) Zoomed in images of IMe-NHC and IMe-NHO, respectively. c, f) A schematic representation of the binding configurations on the Cu(111) surface.

To further deepen our understanding of the binding configurations of IMe-NHO in comparison to IMe-NHC we employed HREELS vibrational measurements. Among other UHV compatible vibrational spectroscopy methods, such as infrared reflection–absorption spectroscopy (IRAS) or helium atom scattering (HAS), HREELS stands out by being able to provide good energy resolution over a wide spectral range with an intrinsic sensitivity to the orientation of vibrational modes relative to the surface via different scattering mechanisms. By comparing specular and off-specular measurements, dipole-active vibrations that possess a dynamic dipole moment perpendicular to the surface can be identified, providing experimental information on the adsorbate orientation.

The obtained spectra are shown in **Figure** 2a,b together with DFT-simulated spectra based on the adsorption geometries which are shown in Figure 2c,d. **Table** 1 also lists the main contributing dipole active modes as well as their assignment based on DFT calculations. For the assignment of vibrational modes, multiple adsorption geometries were considered. However, there were significant discrepancies between the simulated spectra of other adsorption geometries and our experimental results. A more detailed assignment can be found Section 7 in the Supporting Information.

The spectra obtained from IMe-NHC reveal only a single clearly dipole-active signal at 716 cm^{-1}, which is assigned to the C–H wagging of the backbone, consistent with reports on vibrational modes of other NHCs.[57]

The signals at 2972 and 3145 cm^{-1} can be attributed to symmetric and asymmetric C–H stretching vibrations of the methyl groups and the molecular backbone. The features between 1000 and 1500 cm^{-1} correspond to various C–N, C–C, and C=C stretching and C–H bending vibrations

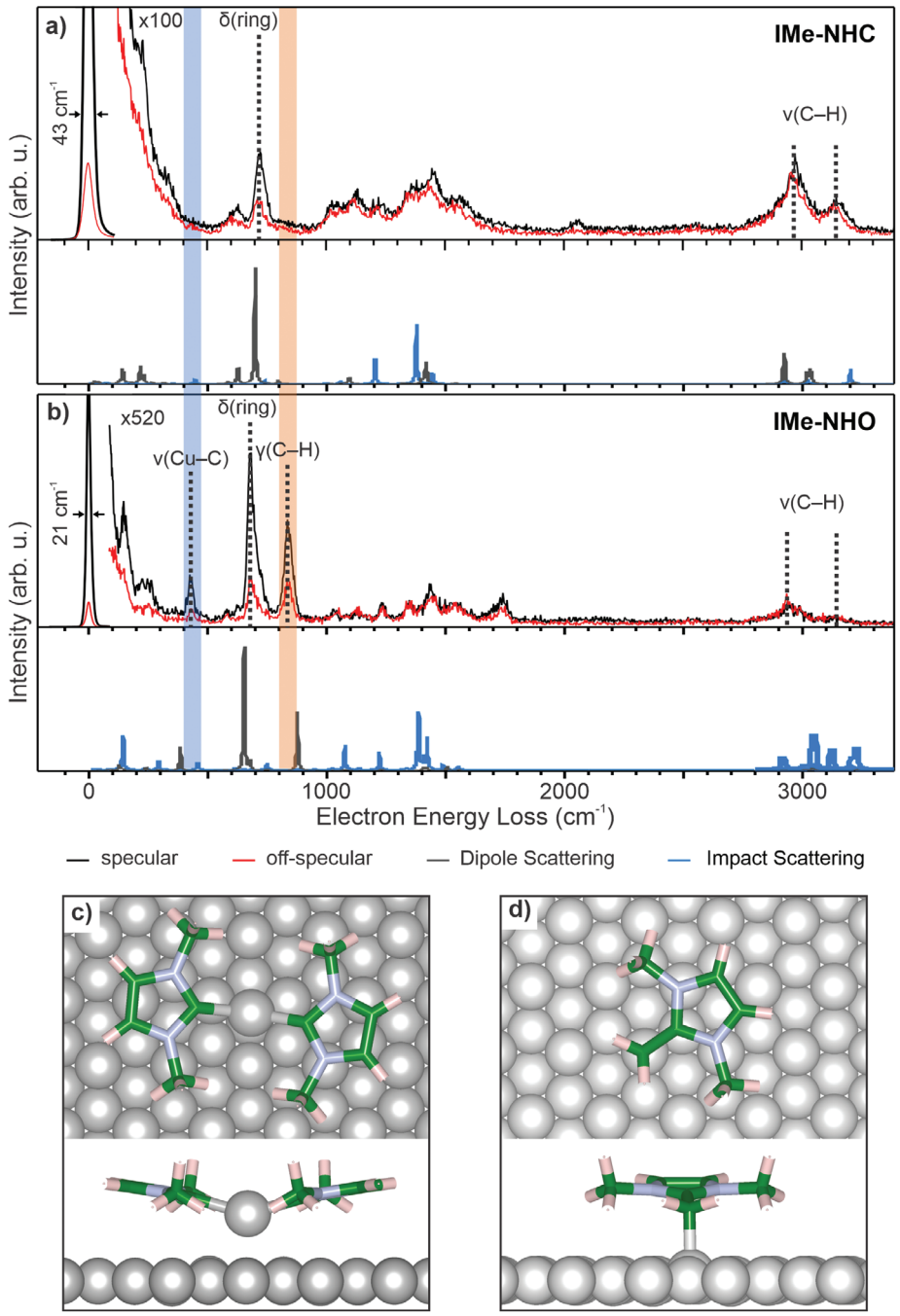

Figure 2. Binding geometry of IMe-NHC and IMe-NHO. Vibrational HREEL spectra in specular (black) and off-specular (red) scattering geometry of sub-monolayer coverages of a) IMe-NHC and b) IMe-NHC together with DFT-calculated intensities and frequencies of the optimized binding geometry produced by impact scattering (blue) and dipole scattering (grey) mechanism. The impact scattered signals were arbitrarily set at 50% of the dipole scattered signal for the highest peak. The off-specular spectra were measured at analyzer angles of either 4.4° (IMe-NHC) or 4.1° (IMe-NHO). The FWHM (full-width at half maximum) of the elastic scattering peak is given as a measurement of resolution. The DFT-optimized binding geometries of c) IMe-NHC ((IMe-NHC)$_2$-Cu$_{ad}$/Cu(111) and d) IMe-NHO ((IMe-NHO)-Cu(111)) each in top-view (top) and side-view (bottom) are also displayed.

of the molecular backbone. The experimental spectrum is in good agreement with the simulated spectra of the (IMe-NHC)$_2$-Cu$_{ad}$/Cu(111) dimer configuration, an adsorption configuration previously reported for this molecule (Figure 2a). In this configuration, the molecular backbone is parallel to the surface and the molecules are bound to a Cu adatom (Figure 2c).

The high relative intensity of the spectrum compared to the dipole-active δ_{ring} vibrations can be explained by the molecule adopting a nonperfectly flat adsorption geometry, binding at an

Table 1. Main dipole active vibrational modes (cm^{-1}) contributing to the HREELS spectra of IMe-NHC and IMe-NHO together with DFT calculated values and the assigned vibrational mode. The abbreviation oop is used for out-of-plane modes.

#	IMe-NHC		IMe-NHO		Mode
	exp.	*theo.*	*exp.*	*theo.*	
I	229	220			buckling
II			425[a)]	381	C–Cu stretching
III	630	625, 630			ring oop-deformation
IV	716[a)]	701-703	677[a)]	650-676	C–H wagging, oop-deformation
V			836[a)]	875	CH_2 wagging
VI	1024	1098			C–H bending
VII	1445	1418	1434	1404	C–H scissoring
VIII			1542	1505	C–C stretch
IX	2972	2922	2941	3042	sym. C–H stretch
X	3145	3027-3035			asym. C–H stretch

[a)] Main peaks visible in the spectra.

angle to the surface plane. This results in vibrations with a dynamic dipole moment in the molecular plane, exhibiting a partial dipole-active character.

Another interpretation is the co-existence of upright and flat-lying species at these low coverages, as reported for similar NHCs with methyl side-chains.[57]

Significant differences are observed in the spectra recorded for IMe-NHO. Three clearly dipole-active vibrations are observed at 425, 677, and 836 cm^{-1}. The first one, marked in blue, is in good agreement with reported ν(NHC-M) metal stretching vibrations.[57–59] The mode is, therefore, assigned to a C–Cu stretching vibration, suggesting a Cu–C bond perpendicular to the surface, indicating a binding geometry with the molecule covalently bound to the surface and the molecular plane parallel to the surface ((IMe-NHO)-Cu(111), Figure 2d).

The other vibrations can be assigned to the ring deformation and C–H wagging mode at 677 cm^{-1} similar to IMe-NHC and a C–H wagging mode at 836 cm^{-1} marked in orange. The latter originates from the terminal CH_2 group which is unique to the IMe-NHO molecule compared to IMe-NHC. These differences in the HREELS spectra support the DFT findings that the NHO molecule chemisorbs on the surface via the ylidic form through a C–Cu bond perpendicular to the surface and with the N-heterocylic backbone parallel to the surface. It further indicates that the NHO remains intact during the evaporation and adsorption process.

The different binding configurations of IMe-NHC and IMe-NHO on Cu(111) is also manifested in their thermal stability. NHCs have been known for their high thermal stability on metal surfaces, a key factor in establishing them as alternatives to thiol-based self-assembled monolayers.[39,58] To establish the thermal stability of the NHO binding configuration in comparison to NHCs, we deposited both molecules on Cu(111) and monitored the molecule density on flat terraces through LT-STM measurements for several annealing steps. The associated images are found in **Figure 3**. IMe-NHC only experiences a small decrease in molecular density until 150 °C. Further annealing leads to a rapid decline in molecule density. At 300 °C, no molecules can be found on the surface and only the step edges of the Cu terraces show minimal organic residue. On the other hand, IMe-NHO shows only minor loss in density all the way up to 200–250 °C before molecules' density sharply drops with increasing temperature. At 350 °C, no molecules can be observed on the Cu terraces. Unlike the IMe-NHC case, more residues can be seen not only at the step edges but also extending onto the terraces. We attribute this behavior to IMe-NHO directly binding to the surface, while IMe-NHC forms the $(IMe\text{-}NHC)_2\text{-}Cu_{ad}$ dimer complexes that are much weaker bound to the surface.

The different binding mode of the NHO molecule also raises the question of how it influences the charge transfer during the binding process. NHO ligands have been found to be stronger electron donors as compared to NHCs in transition metal complexes, which is remarkable considering that NHCs themselves are known for their strong electron-donating capabilities.[16,17]

To investigate whether this holds true on a Cu(111) surface, we have employed C1s and N1s XPS measurements, as the binding energy is directly related to the electron density.

For IMe-NHC, XPS data exist for multiple surfaces including Si(111),[46] Au(111),[37,38] and Cu(111).[37] Studies by Franz et al. demonstrated that the electron transfer from IMe-NHC to the substrate is very similar on Au(111) (0.29 *e*) and Si(111) (0.26 *e*).[46]

Our calculated Bader charges evidence a very small charge transfer from IMe-NHC to Cu(111) (0.13 *e*). Additionally, Jiang et al.[37] have shown that the C1s XPS spectra for IMe-NHC are virtually identical when comparing Au(111) and Cu(111). These findings suggest a similar amount of electron transfer on Cu(111).

The C1s XPS spectra of IMe-NHC and IMe-NHO on Cu(111) are shown in **Figure 4a** and b, respectively. Annealing to 100 °C prior to XPS measurements to remove any physisorbed species resulted in a slight sharpening and minor shift of the N1s peak but significant change in the C1s peak. The spectrum of IMe-NHC shows a single peak at 286.4 eV with a slight asymmetry on the lower binding energy side. In contrast, the spectrum of IMe-NHO shows a peak with a significant shoulder on the lower binding energy side and the main peak is shifted significantly to 287.2 eV compared to IMe-NHC. This already indicates a significant difference in the electronic structure upon binding of IMe-NHO compared to IMe-NHC. The appearance of the C1s peak is in agreement with C1s data published for IMe-NHO adsorbed on Au(111)[52] and Si(111).[51]

Further analysis involves deconvoluting the C1s XPS spectra. Because resolution of the C1s spectra is limited due to the nonmonochromated X-ray source, DFT calculated peak positions have been used to deconvolute the spectra. The spectrum of IMe-NHC (Figure 4a) can be separated into the expected three signals for the molecule. The C_1 and C_2 signals are found at 286.5 and 285.7 eV, respectively, in good agreement with literature values of carbon atoms bonded to N atoms.

The surface-bound carbene C_3 atom is observed at 287.2 eV, which corresponds to a C atom bound to two N atoms. In this literature, this is attributed to a shift of +1 to 1.5 eV compared to C atoms bound to one N atom.[37]

The spectra of IMe-NHO (Figure 4b) exhibit noticeable differences compared to IMe-NHC.

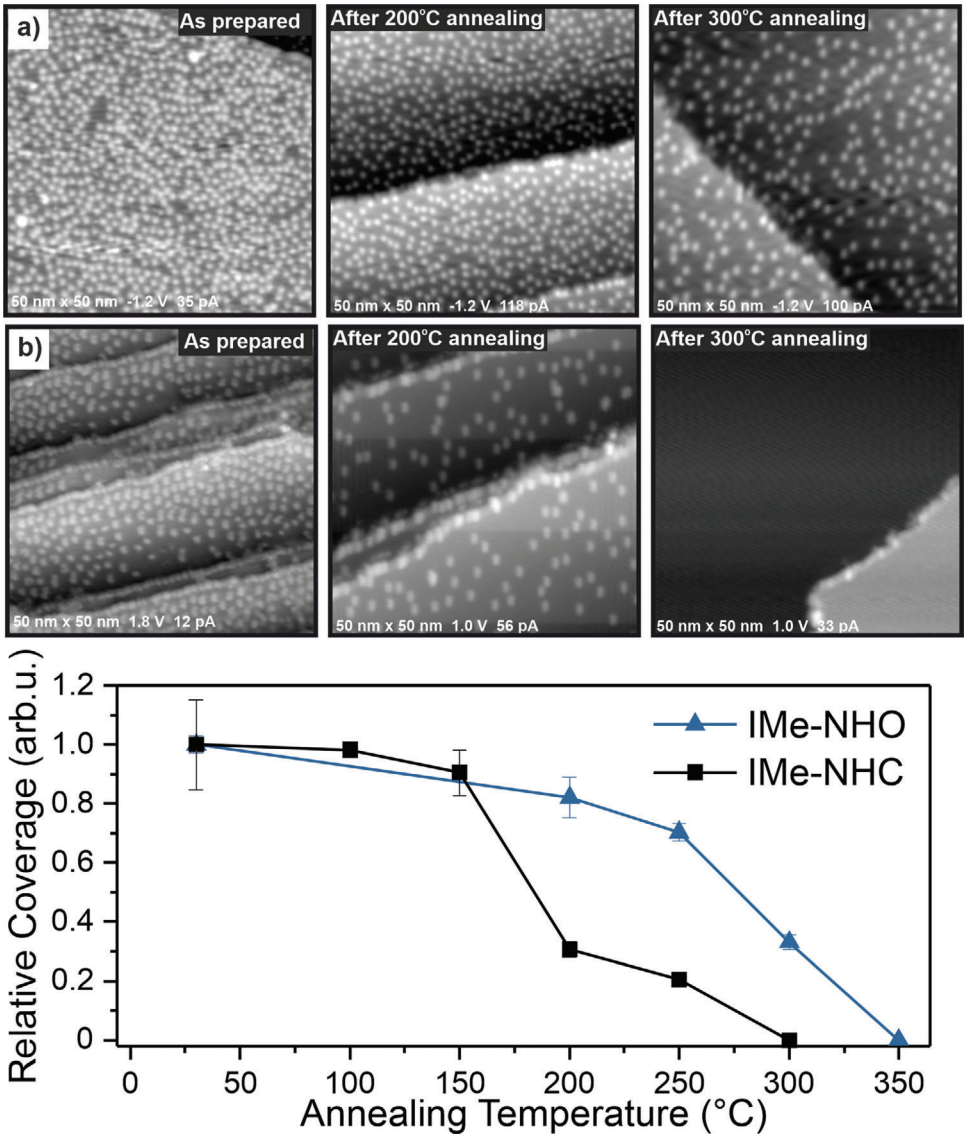

Figure 3. LT-STM images of a) IMe-NHO and b) IMe-NHC on Cu(111) after successive annealing steps at different annealing temperatures. Below a quantitative analysis of the coverage behavior of IMe-NHC and IMe-NHO on Cu(111) depending on annealing temperature is plotted. The images and corresponding coverages were taken by consecutively annealing the initially prepared surface for 60 s at each temperature step. Intermediate steps can be found in Figure S6, Supporting Information.

The C_3 peak is shifted to 288.5 eV due to the absence of a metal center, while the new metal-bound C_4 appears at 284.7 eV. The C_1 and C_2 signals are found at 287.1 and 285.9 eV, respectively. The observed shifts are in qualitative agreement with initial state core level shift calculations, and the shifts with respect to the C_1 of IMe-NHC are summarized in **Table 2**. It should be noted that while the deconvolution into the individual components are prone to a fitting error, the main peak positions show the same trend with a significant difference of 0.8 eV between IMe-NHC and IMe-NHO that is not affected by the fitting error.

Interestingly, a shift to higher binding energy can be observed for C_1 when going from IMe-NHC to IMe-NHO. This shift indicates a lower electron density in the imidazole ring for IMe-NHO compared to IMe-NHC. This conclusion is further supported by the N1s XPS spectra (Figure 4c), where an increase from 401.1 eV for IMe-NHC to 401.2 eV for IMe-NHO can be observed. This observation is in accordance with previous studies of IMe-NHC and IMe-NHO on Au(111) and a modified Si(111) surface where a N1s shift from 401.2 to 402.2 eV and 401.0 to 402.1 eV has been observed.[51,52]

A DFT analysis of the Bader charges supports the shift in electron density, demonstrating that the net electron transfer from IMe-NHO to the surface is more than that of IMe-NHC (0.33 *e* compared to 0.13 *e*), which has already been shown to transfer electron density upon binding to well-prepared Si and Au surfaces.[46] This not only provides additional evidence for the bond of the ylidic form of IMe-NHO to the Cu(111) surface but also highlights the potential of the NHO compound class as a

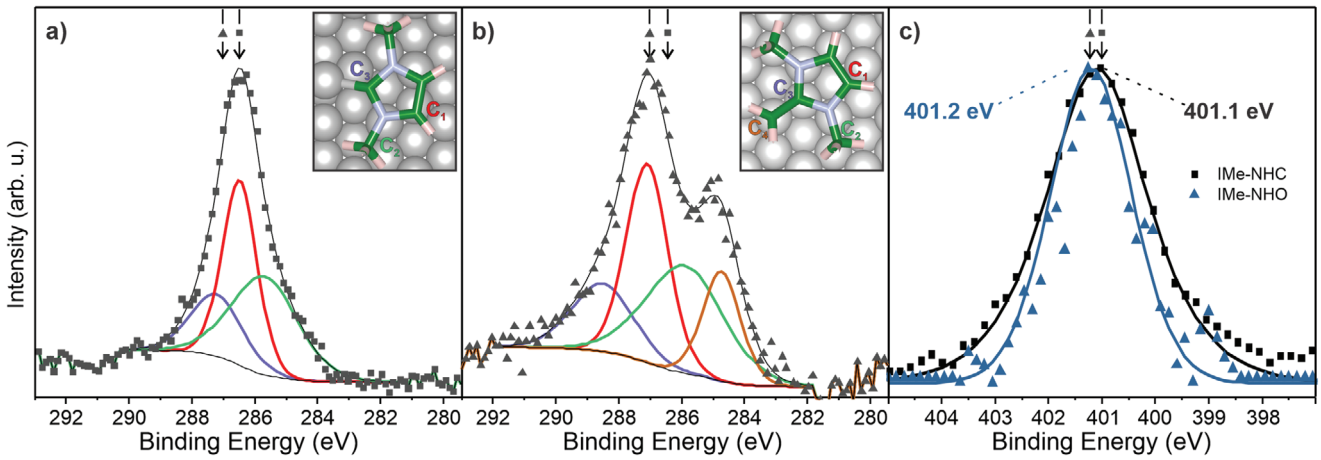

Figure 4. C1s and N1s XPS spectra of IMe-NHC and IMe-NHO. Fitted C1s XPS peaks of a) IMe-NHC and b) IMe-NHO. The underlying subspectral peaks are area-constrained to reflect stoichiometric ratios 2:2:1 and 2:2:1:1, respectively. The main peaks are located at 286.4 and 287.2 eV, respectively. Their positions have been marked in both graphs. c) Background-subtracted and intensity normalized N1s XPS spectra of IMe-NHC (black) and IMe-NHO (blue) on Cu(111). The respective peak positions have been marked in the graphs.

whole for surface modifications. The almost cationic character observed is an inherent property confined to the surface, arising from charge separation upon binding and the subsequent "lock-in" of the ylidic form due to the separation of the π-system of the molecular backbone from the surface. This property distinguishes NHOs from well-established NHCs and could provide a complementary method for modifying surfaces using organic molecules.

An increased charge donation from the adsorbed molecules to the Cu surface could affect a change of the work function. To investigate this aspect, we measured the secondary electron onsets for Cu(111) surfaces with different coverages of IMe-NHO and IMe-NHC (Figure S7h, Supporting Information). The resulting reduction in the work function can be seen in **Figure 5**a. In Figure 5b, the DFT calculated work functions for the (IMe-NHO)-Cu(111), (IMe-NHC)-Cu(111) and the (IMe-NHC)$_2$-Cu$_{ad}$/Cu(111) configuration are displayed.

For a given coverage, the shift in the wok function is higher for IMe-NHO than for IMe-NHC. This observation is in agreement with a higher net electron transfer to the surface for IMe-NHO, leading to an increased dipole moment perpendicular to the surface compared to IMe-NHC (Table S2, Supporting Information) and subsequently a higher shift in work function. Note that for the upright binding configuration (IMe-NHC)-Cu(111), the change in dipole moment perpendicular to the surface and the subsequent work function shift would be expected to be very similar to the (IMe-NHO)-Cu(111) configuration.

Table 2. Experimentally and theoretically determined B.E. positions of the C1s and N1s peaks for IMe-NHC and IMe-NHO on Cu(111). For easy comparison, the values for the C_1 of IMe-NHC have been aligned. All other values are given in relation to the C_1 values and N_1, respectively. All shifts are given in units of eV. The absolute values can be found in Table S1, Supporting Information.

	IMe-NHC	IMe-NHO	IMe-NHC	IMe-NHO
	(*exp.*)[a]		(*theo.*)[b]	
C_1	0	+ 0.6	0	+ 0.1
C_2	− 0.8	− 0.6	− 0.1	0
C_3	+ 0.7	+ 2.0	+ 0.5	+ 1.5
C_4	–	− 1.8	–	− 1.1
N	0	+ 0.1	0	+ 0.2

[a] Values referenced to IMe-NHC (*exp.*) C_1 and N_1; [b] Values referenced to IMe-NHC (*theo.*) C_1 and N_1.

3. Conclusion

In this study, we investigated the adsorption properties of submonolayer coverages of the sterically low-demanding IMe-NHO on a well-defined Cu(111) surface under UHV conditions and compared it to the respective IMe-NHC derivative.

Our HREELS data clearly demonstrated that IMe-NHO chemisorbs to the Cu(111) surface "via" a C–Cu bond perpendicular to the surface. Both IMe-NHO and IMe-NHC adsorb with their N-heterocyclic backbones parallel to the surface. Moreover, both IMe-NHO and IMe-NHC did not show any short-range or long-range order on the surface at the investigated submonolayer coverage, as revealed by LT-STM measurements.

One of the significant findings of this study is that the net electron transfer from the molecule to the surface is significantly higher for IMe-NHO compared to IMe-NHC, as evidenced by the higher binding energies observed in the C1s and N1s XPS data. This is noteworthy considering the well-established status of NHCs as strong electron donors in surface science.

These differences in adsorption between IMe-NHC and IMe-NHO lead to a stronger adsorption to the surface of IMe-NHO and a resulting increased thermal stability. Moreover, IMe-NHO induces a stronger reduction of the surfaces' work function. These findings suggest that NHOs could be viable alternatives to NHCs in surface modification research.

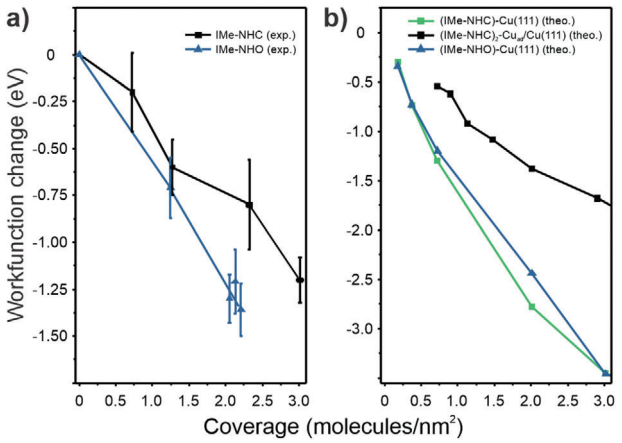

Figure 5. a) Experimentally determined work function reduction for layers of IMe-NHC and IMe-NHO with varying coverage. b) Calculated values of work function reduction for layers of IMe-NHC and IMe-NHO with varying coverage. For IMe-NHC, two different adsorption geometries were considered.

4. Experimental Section

Molecule Synthesis: Detailed synthetic procedure and characterization for the CO_2-adduct of IMe-NHO is included in the Supporting Information section.

Sample Preparation: As precursor for IMe-NHC, bench-stable 1,3-dimethyl-1*H*-imidazol-3-ium-2-carboxylate (IMe-NHC-CO_2) was used that is known to generate the free IMe-NHC under heating in ultrahigh vacuum with only gaseous CO_2 as a by-product, enabling a clean NHC deposition on the surface. For IMe-NHO, a similar route was employed, using 1,3-dimethyl-1*H*-imidazol-3-ium-2-yl-acetate (IMe-NHO-CO_2) as a precursor. For details on the synthesis and characterization by nuclear magnetic resonance spectroscopy, see Section 1 in the Supporting Information. The Cu surfaces (99.99 %, MaTeck) were prepared in UHV chambers with a background pressure $<5 \times 10^{-10}$ mbar combining Ar^+ bombardment cycles at 1 kV and annealing at 900–950 K. The molecules were evaporated from a heated quartz crucible in a "Kentax" evaporator at 318–328 K.

Computational Methods: All calculations were done with the code VASP 6.[60,61] The core electrons were modeled with the Projector Augmented Wave (PAW) method,[62,63] while H(1s), C(2s,2p), N(2s,2p), O(2s,2p) and Cu(3d,4s) electrons were treated explicitly with a set of plane waves expanded up to a kinetic energy cutoff of 400 eV. The PBE exchange-correlation functional[64] was adopted, including the long-range dispersion according to the DFT+D2′ scheme.[65,66] The IMe-NHC-Cu-IMe-NHC dimer structure (Figure S4, Supporting Information) was generated by adding an extra-lattice Cu atom on a three-folded hollow site on Cu(111). The adsorption energy, D_e, was defined as the energy of the molecule/substrate adduct with respect to the energy of its separated components:

$$D_e = E(\text{IMe-NHX/Cu}) - [E(\text{IMe-NHX}) + E(\text{Cu})] \quad (1)$$

where IMe-NHX stands for either IMe-NHC or IMe-NHO. Negative values of D_e imply stable bonding. In the case of dimers, D_e is reported per molecule. Further details on the numerical tolerances, the construction of the supercells, and the simulation of the vibrational spectra are reported in the Supporting Information.

UHV Techniques: LT-STM measurements were conducted in a self-designed low-temperature scanning tunneling microscope operating at 5 K using a PtIr tip. HREELS measurements were conducted at T < 80 K in a Delta 0.5 (VSI) spectrometer. The recorded spectra exhibited a full width at half-maximum resolution of < 36 cm^{-1} (4.5 meV) for the elastic peak in specular geometry. XPS measurements were performed using a SPECS X-ray source with an Al anode operating at 300 W and a Phoibos100 analyzer. The background of the spectra were subtracted through the Shirley method. For the fittings, Gaussian–Lorentzian functions were used. Further experimental details can be found in Section 1 in the Supporting Information.

Supporting Information

Supporting Information is available from the Wiley Online Library or from the author.

Acknowledgements

F.L., M.D., and S.T. contributed equally to this work. F.L., J.J.N., and M.H. thank Helmut Kuhlenbeck for advice on experimental HREELS setup and scientific discussion. J.J.N. thanks the Alexander von Humboldt Foundation for the generous financial support. S.T. and G.P. acknowledge the financial support from the Italian Ministry of University and Research (MIUR) through the PRIN Project 20179337R7. S.T. and G. P. acknowledge the access to the CINECA supercomputing resources was granted via ISCRAB program. F.G., M.D., A.D., and M.K. gratefully acknowledge generous financial support of the Deutsche Forschungsgemeinschaft (SFB 858 and SFB 1459) and through the International Graduate School for Battery Chemistry, Characterization, Analysis, Recycling and Application (BACCARA), funded by the Ministry for Culture and Science of North Rhine Westphalia, Germany.

Conflict of Interest

The authors declare no conflict of interest.

Data Availability Statement

The data that support the findings of this study are available from the corresponding author upon reasonable request.

Keywords

high-resolution electron energy-loss spectroscopy, N-heterocyclic carbenes, N-heterocyclic olefins, scanning tunneling microscopy, X-ray photoemission spectroscopy

Received: May 2, 2024
Published online:

[1] E. Ericsson, T. Marnung, J. Sandstörm, I. Wennerbeck, *J. Mol. Struct.* **1975**, *24*, 373.
[2] S. Naumann, *Chem. Commun.* **2019**, *55*, 11658.
[3] M. M. D. Roy, E. Rivard, *Acc. Chem. Res.* **2017**, *50*, 2017.
[4] A. Doddi, M. Peters, M. Tamm, *Chem. Rev.* **2019**, *119*, 6994.
[5] R. Dorta, E. D. Stevens, N. M. Scott, C. Costabile, L. Cavallo, C. D. Hoff, S. P. Nolan, *J. Am. Chem. Soc.* **2005**,*127*, 2485.
[6] N. Kuhn, H. Bohnen, J. Kreutzberg, D. Bläser, R. Boese, *J. Chem. Soc., Chem. Commun.* **1993**, *184*, 1136.
[7] N. Kuhn, M. Steimann, G. Weyers, *Zeitschrift fur Naturforsch. - Sect. B J. Chem. Sci.* **1999**, *54*, 427.
[8] A. Dumrath, X.-F. Wu, H. Neumann, A. Spannenberg, R. Jackstell, M. Beller, *Angew. Chem. Int. Ed.* **2010**, *49*, 8988.

[9] Y.-B. Wang, D.-S. Sun, H. Zhou, W.-Z. Zhang, X.-B. Lu, *Green Chem.* **2015**, *17*, 4009.
[10] I. C. Watson, A. Schumann, H. Yu, E. C. Davy, R. McDonald, M. J. Ferguson, C. Hering-Junghans, E. Rivard, *Chem. - A Eur. J.* **2019**, *25*, 9678.
[11] A. T. Biju, M. Padmanaban, N. E. Wurz, F. Glorius, *Angew. Chem. Int. Ed.* **2011**, *50*, 8412.
[12] B. Maji, M. Horn, H. Mayr, *Angew. Chem. Int. Ed.* **2012**, *51*, 6231.
[13] B. Maji, H. Mayr, *Angew. Chem. Int. Ed.* **2012**, *51*, 10408.
[14] C. E. I. Knappke, J. M. Neudörfl, A. J. von Wangelin, *Org. Biomol. Chem.* **2010**, *8*, 1695.
[15] M. Schedler, N. E. Wurz, C. G. Daniliuc, F. Glorius, *Org. Lett.* **2014**, *16*, 3134.
[16] A. Fürstner, M. Alcarazo, R. Goddard, C. W. Lehmann, *Angew. Chem. Int. Ed.* **2008**, *47*, 3210.
[17] K. Powers, C. Hering-Junghans, R. McDonald, M. J. Ferguson, E. Rivard, *Polyhedron* **2016**, *108*, 8.
[18] M. N. Hopkinson, C. Richter, M. Schedler, F. Glorius, *Nature* **2014**, *510*, 485.
[19] P. Bellotti, M. Koy, M. N. Hopkinson, F. Glorius, *Nat. Rev. Chem.* **2021**, *5*, 711.
[20] C. A. Smith, M. R. Narouz, P. A. Lummis, I. Singh, A. Nazemi, C.-H. Li, C. M. Crudden, *Chem. Rev.* **2019**, *119*, 4986.
[21] M. Koy, P. Bellotti, M. Das, F. Glorius, *Nat. Catal.* **2021**, *4*, 352.
[22] E. Amit, L. Dery, S. Dery, S. Kim, A. Roy, Q. Hu, V. Gutkin, H. Eisenberg, T. Stein, D. Mandler, F. Dean Toste, E. Gross, *Nat. Commun.* **2020**, *11*, 5714.
[23] J. B. Ernst, C. Schwermann, G.-i. Yokota, M. Tada, S. Muratsugu, N. L. Doltsinis, F. Glorius, *J. Am. Chem. Soc.* **2017**, *139*, 9144.
[24] K. V. S. Ranganath, J. Kloesges, A. H. Schäfer, F. Glorius, *Angew. Chem. Int. Ed.* **2010**, *49*, 7786.
[25] P. Knecht, D. Meier, J. Reichert, D. A. Duncan, M. Schwarz, J. T. Küchle, T. Lee, P. S. Deimel, P. Feulner, F. Allegretti, W. Auwärter, G. Médard, A. P. Seitsonen, J. V. Barth, A. C. Papageorgiou, *Angew. Chem.* **2022**, *134*, 1.
[26] I. Berg, L. Hale, M. Carmiel-Kostan, F. D. Toste, E. Gross, *Chem. Commun.* **2021**, *57*, 5342.
[27] D. T. Nguyen, M. Freitag, M. Körsgen, S. Lamping, A. Rühling, A. H. Schäfer, M. H. Siekman, H. F. Arlinghaus, W. G. van der Wiel, F. Glorius, B. J. Ravoo, *Angew. Chem. Int. Ed.* **2018**, *57*, 11465.
[28] C.-Y. Wu, W. J. Wolf, Y. Levartovsky, H. A. Bechtel, M. C. Martin, F. D. Toste, E. Gross, *Nature* **2017**, *541*, 511.
[29] G. Kaur, R. L. Thimes, J. P. Camden, D. M. Jenkins, *Chem. Commun.* **2022**, *58*, 13188.
[30] E. A. Doud, M. S. Inkpen, G. Lovat, E. Montes, D. W. Paley, M. L. Steigerwald, H. Vázquez, L. Venkataraman, X. Roy, *J. Am. Chem. Soc.* **2018**, *140*, 8944.
[31] R. J. Lewis, M. Koy, M. Macino, M. Das, J. H. Carter, D. J. Morgan, T. E. Davies, J. B. Ernst, S. J. Freakley, F. Glorius, G. J. Hutchings, *J. Am. Chem. Soc.* **2022**, *144*, 15431.
[32] Y. Choi, C. S. Park, H.-V. Tran, C.-H. Li, C. M. Crudden, T. R. Lee, *ACS Appl. Mater. Interfaces* **2022**, *14*, 44969.
[33] Z. Li, K. Munro, I. I. Ebralize, M. R. Narouz, J. D. Padmos, H. Hao, C. M. Crudden, J. H. Horton, *Langmuir* **2017**, *33*, 13936.
[34] A. V. Zhukhovitskiy, M. G. Mavros, T. Van Voorhis, J. A. Johnson, *J. Am. Chem. Soc.* **2013**, *135*, 7418.
[35] A. V. Zhukhovitskiy, M. J. MacLeod, J. A. Johnson, *Chem. Rev.* **2015**, *115*, 11503.
[36] G. Wang, A. Rühling, S. Amirjalayer, M. Knor, J. B. Ernst, C. Richter, H.-J. Gao, A. Timmer, H.-Y. Gao, N. L. Doltsinis, F. Glorius, H. Fuchs, *Nat. Chem.* **2017**, *9*, 152.
[37] L. Jiang, B. Zhang, G. Médard, A. P. Seitsonen, F. Haag, F. Allegretti, J. Reichert, B. Kuster, J. V. Barth, A. C. Papageorgiou, *Chem. Sci.* **2017**, *8*, 8301.
[38] A. Bakker, A. Timmer, E. Kolodzeiski, M. Freitag, H. Y. Gao, H. Mönig, S. Amirjalayer, F. Glorius, H. Fuchs, *J. Am. Chem. Soc.* **2018**, *140*, 11889.
[39] C. M. Crudden, J. H. Horton, I. I. Ebralidze, O. V. Zenkina, A. B. McLean, B. Drevniok, Z. She, H.-B. Kraatz, N. J. Mosey, T. Seki, E. C. Keske, J. D. Leake, A. Rousina-Webb, G. Wu, *Nat. Chem.* **2014**, *6*, 409.
[40] A. Inayeh, R. R. K. Groome, I. Singh, A. J. Veinot, F. C. de Lima, R. H. Miwa, C. M. Crudden, A. B. McLean, *Nat. Commun.* **2021**, *12*, 4034.
[41] M. J. Trujillo, S. L. Strausser, J. C. Becca, J. F. DeJesus, L. Jensen, D. M. Jenkins, J. P. Camden, *J. Phys. Chem. Lett.* **2018**, *9*, 6779.
[42] E. A. Doud, R. L. Starr, G. Kladnik, A. Voevodin, E. Montes, N. P. Arasu, Y. Zang, P. Zahl, A. Morgante, L. Venkataraman, H. Vázquez, D. Cvetko, X. Roy, *J. Am. Chem. Soc.* **2020**, *142*, 19902.
[43] A. Krzykawska, M. Wróbel, K. Kozieł, P. Cyganik, *ACS Nano* **2020**, *14*, 6043.
[44] G. Lovat, E. A. Doud, D. Lu, G. Kladnik, M. S. Inkpen, M. L. Steigerwald, D. Cvetko, M. S. Hybertsen, A. Morgante, X. Roy, L. Venkataraman, *Chem. Sci.* **2019**, *10*, 930.
[45] M. R. Narouz, K. M. Osten, P. J. Unsworth, R. W. Y. Man, K. Salorinne, S. Takano, R. Tomihara, S. Kaappa, S. Malola, C.-T. Dinh, J. D. Padmos, K. Ayoo, P. J. Garrett, M. Nambo, J. H. Horton, E. H. Sargent, H. Häkkinen, T. Tsukuda, C. M. Crudden, *Nat. Chem.* **2019**, *11*, 419.
[46] M. Franz, S. Chandola, M. Koy, R. Zielinski, H. Aldahhak, M. Das, M. Freitag, U. Gerstmann, D. Liebig, A. K. Hoffmann, M. Rosin, W. G. Schmidt, C. Hogan, F. Glorius, N. Esser, M. Dähne, *Nat. Chem.* **2021**, *13*, 828.
[47] J. J. Navarro, M. Das, S. Tosoni, F. Landwehr, M. Koy, M. Heyde, G. Pacchioni, F. Glorius, B. Roldan Cuenya, *Angew. Chem. Int. Ed.* **2022**, *61*, 202202127.
[48] J. J. Navarro, M. Das, S. Tosoni, F. Landwehr, J. P. Bruce, M. Heyde, G. Pacchioni, F. Glorius, B. Roldan Cuenya, *J. Am. Chem. Soc.* **2022**, *144*, 16267.
[49] J. J. Navarro, M. Das, S. Tosoni, F. Landwehr, M. Heyde, G. Pacchioni, F. Glorius, B. Roldan Cuenya, *J. Phys. Chem. C* **2022**, *126*, 17528.
[50] I. Berg, E. Amit, L. Hale, F. D. Toste, E. Gross, *Angew. Chem. Int. Ed.* **2022**, *w61*, 202201093.
[51] I. Berg, L. Schio, J. Reitz, E. Molteni, C. G. Bolaños, A. Goldoni, G. Fratesi, M. M. Hansmann, L. Floreano, *Angew. Chem. Int. Ed.* **2023**, *62*, 202311832.
[52] M. Das, C. Hogan, R. Zielinski, M. Kubicki, M. Koy, C. Kosbab, S. Brozzesi, A. Das, M. T. Nehring, V. Balfanz, J. Brühne, M. Dähne, M. Franz, N. Esser, F. Glorius, *Angew. Chem. Int. Ed.* **2023**, *62*, 202314663.
[53] J. Rickerby, J. H. G. Steinke, *Chem. Rev.* **2002**, *102*, 1525.
[54] W. Wang, C. Deng, S. Xie, Y. Li, W. Zhang, H. Sheng, C. Chen, J. Zhao, *J. Am. Chem. Soc.* **2021**, *143*, 2984.
[55] S. Nitopi, E. Bertheussen, S. B. Scott, X. Liu, A. K. Engstfeld, S. Horch, B. Seger, I. E. L. Stephens, K. Chan, C. Hahn, J. K. Nørskov, T. F. Jaramillo, I. Chorkendorff, *Chem. Rev.* **2019**, *119*, 7610.
[56] R. M. Bullock, J. G. Chen, L. Gagliardi, P. J. Chirik, O. K. Farha, C. H. Hendon, C. W. Jones, J. A. Keith, J. Klosin, S. D. Minteer, R. H. Morris, A. T. Radosevich, T. B. Rauchfuss, N. A. Strotman, A. Vojvodic, T. R. Ward, J. Y. Yang, Y. Surendranath, *Science* **2020**, *369*.
[57] C. R. Larrea, C. J. Baddeley, M. R. Narouz, N. J. Mosey, J. H. Horton, C. M. Crudden, *ChemPhysChem* **2017**, *18*, 3536.
[58] C. M. Crudden, J. H. Horton, M. R. Narouz, Z. Li, C. A. Smith, K. Munro, C. J. Baddeley, C. R. Larrea, B. Drevniok, B. Thanabalasingam,

A. B. McLean, O. V. Zenkina, I. I. Ebralidze, Z. She, H.-B. Kraatz, N. J. Mosey, L. N. Saunders, A. Yagi, *Nat. Commun.* **2016**, *7*, 12654.
[59] E. Angove, F. Grillo, H. A. Früchtl, A. J. Veinot, I. Singh, J. H. Horton, C. M. Crudden, C. J. Baddeley, *J. Phys. Chem. Lett.* **2022**, *13*, 2051.
[60] G. Kresse, J. Furthmüller, *Comput. Mater. Sci.* **1996**, *6*, 15.
[61] G. Kresse, J. Furthmüller, *Phys. Rev. B* **1996**, *54*, 11169.
[62] P. E. Blöchl, *Phys. Rev. B* **1994**, *50*, 17953.
[63] G. Kresse, D. Joubert, *Phys. Rev. B* **1999**, *59*, 1758.
[64] J. P. Perdew, K. Burke, M. Ernzerhof, *Phys. Rev. Lett.* **1996**, *77*, 3865.
[65] S. Grimme, *J. Comput. Chem.* **2006**, *27*, 1787.
[66] S. Tosoni, J. Sauer, *Phys. Chem. Chem. Phys.* **2010**, *12*, 14330.